Contents lists available at ScienceDirect

Applied Energy

journal homepage: http://ees.elsevier.com

A spectral-splitting photovoltaic-thermochemical system for energy storage and solar power generation

Yunyi Ling [a,b], Wenjia Li [a,b], Jian Jin [a,b], Yuhang Yu [c], Yong Hao [a,b], Hongguang Jin [a,b]

[a] Institute of Engineering Thermophysics, Chinese Academy of Sciences, Beijing 100190, PR China
[b] University of Chinese Academy of Sciences, Beijing 100049, PR China
[c] Department of Thermal Science and Energy Engineering, University of Science and Technology of China, Hefei 230027, PR China

ARTICLE INFO

Keywords
Solar thermochemical
Photovoltaic
Hybrid system
Spectrally selective filter
Efficiency

ABSTRACT

A hybrid solar energy conversion and storage system integrating a CdTe solar cell and methanol thermochemistry with a spectral filter assigning different parts of the solar spectrum is proposed. A thermodynamic model and an optical model are established to study the photovoltaic and thermal performance of this system. The results show that the system features high solar power generation efficiency (up to 39%) and good potential for solar thermal energy storage (up to 60%) as a result of both spectral filtering and the manipulation of individual linear Fresnel reflectors, which also considerably enhance control flexibility. Sensitivity analysis shows that the system remains highly effective in solar to power conversion against non-ideal conditions. The economic assessment indicates that the levelized cost of electricity is as low as $ 0.20/kWh.

1. Introduction

The combination of solar photovoltaic (PV) and solar thermal energy conversion approaches, known as PVT, is an intensively studied area in solar energy technologies [1]. PVT hybrid system utilizes solar energy through two components, i.e., PV system and thermal system in series. PV system converts sunlight into electricity, and thermal system utilizes heat from PV cell(s) in a specific end-user application, such as space heating, direct hot water [2], or cooling [3]. This cascaded utilization enables higher overall theoretical efficiency than PV system or thermal system alone. To further improve the quality of the thermal energy, concentrators are required to intensify the solar flux; such systems are called CPVT systems. The configuration and performance of CPVT systems have recently been reviewed by Sharaf and Orhan [4,5]. In a CPVT system, the temperature of the extracted heat reaches up to 200–300 °C, and this mid/low-temperature thermal energy can be utilized for a wide variety of purposes, such as power generation [6,7], seawater desalination [8], air conditioning [9], and cooling [10,11]. To allow these conventional CPVT systems to achieve respectable efficiencies, synergistic coupling between PV power generation and thermal energy conversion (to various forms, including power) is crucial. However, an essential challenge of such combinations is that the temperature of PV cells directly sets the upper limit of the thermodynamic cycle for the purpose of thermal energy conversion in the thermal system. Additionally, due to the adverse temperature coefficient (for power generation) and tolerance to elevated temperature of PV cells, the selection of PV cells is severely limited, and the efficiency of converting thermal energy to useful work is also severely limited. Numerous studies have demonstrated difficulties in achieving considerable improvement of the solar-to-work efficiency on the basis of PV cells alone [12,13].

Compared with the thermal-only utilization approaches above, thermochemistry may be a more effective means of achieving solar-to-work conversion. In this method, thermal energy is utilized to drive endothermic chemical reaction instead of heat engine as discussed above. Hong and Jin proposed an efficient solar thermochemical power system integrated with methanol decomposition ($CH_3OH(g) \rightarrow CO(g) + 2H_2(g)$, $\Delta H^{\Theta}_{200\,^{\circ}C} = 896.8\,kJ\,mol^{-1}$) [14,15], with a net-solar-electric (NSE) efficiency that reaches 35%. With this work as a starting point, our group have performed investigations of concentrated solar photovoltaic-thermochemical energy conversion systems. Li et al. proposed several CPVT hybrid systems combining methanol decomposition and PV power generation based on various concentrating techniques, such as parabolic trough [16] and point-focus Fresnel concentrator [17]. In these systems, multi-junction solar cells were employed for power generation. Thermodynamic analysis indicated that these systems were characterized by NSE efficiency over 40% (compared with 28% for PV cells alone), and meanwhile featured easy energy storage and flexible application scalability. Compared with previous work on CPVT systems in the literature, good improvements were achieved

https://doi.org/10.1016/j.apenergy.2019.113631
Received 17 December 2018; Received in revised form 15 July 2019; Accepted 29 July 2019
Available online xxx
0306-2619/

in both NSE efficiency and its net increase on the basis of the PV module alone. The fundamental reason for these improvements is that the upper limit of temperature of the thermodynamic cycle (and thus the upper limit of the efficiency of the thermodynamic cycle) is no longer bound by the temperature of the PV module. By contrast, the correlation in temperature between the PV and thermal (or more precisely, thermochemical) modules of the systems remains strong; the methanol decomposition reaction over the conventional $CuO/ZnO/Al_2O_3$ catalyst requires temperatures of 200–250 °C, which pushes on the upper temperature limit of PV cells. Few PV cells (e.g., multijunction GaAs cells) can tolerate such extreme temperatures, and all of them are costly ($ 35000/m^2 for multi-junction GaAs cells [18]), and nearly all commercialized cost-effective PV cells (e.g., Si-cased cells and CdTe thin film cells) will be damaged in this temperature range. From a practical point of view, in addition to disconnecting the temperature correlation, challenges such as the cost of hybrid systems, the integration of PV cells and heat-collection modules, the range of selection of PV cells, and the type of fossil fuels used for the thermochemical module remain daunting tasks that require innovative solutions.

Spectral filter, a device that selectively assigns light by reflection, transmission or absorption on the basis of their responses to different parts of spectrum, may offer a potential solution to these problems. For example, as one of the most commonly used spectral filters, ultraviolet (UV) filters absorb ultraviolet radiation, but let visible light through. By applying a spectral filter to a CPVT system, it is viable to allocate the PV-suitable short wavelength to the PV system. Photonic energy with longer wavelengths (than that needed for PV) could be redirected to the thermal module to supply heat directly, and the PV cell would no longer be attached to the thermal part, allowing these two systems to work under separate temperatures. The notion of this method was first proposed by Jackson in 1955 [19], and this triggered a large amount of scientific studies, especially in recent years. Imenes [20], Mojiri [21] and Ju [22] have reviewed CPVT hybrid systems based on spectral-splitting technology extensively. Segal investigated the feasibility of implementing spectral splitting in solar power towers to cogenerate electricity and heat, and the optical issue was thoroughly studied, especially the heliostat field layout [23]. Hu numerically studied the optical and thermodynamic performance of a CPVT hybrid system with a spectral filter and fully tracked linear Fresnel reflector concentrators [24]. Kandilli proposed a concentrating photovoltaic combined system using a dish concentrator in which thermal energy was utilized for domestic heating [25]. Chen published a study of a hybrid electric and thermal solar receiver composed of transparent silica aerogel and spectrally selective light pipe with solar-electricity-efficiency over 35% [26]. As seen from the studies above, the separation of the PV and thermal modules opens up possibilities of attaining temperatures beyond the tolerance threshold of all PV cells, which is beneficial for the conversion of a wider range of fossil fuels. This optimized matching between the PV cell's spectral response and the spectral profile of the incident solar radiation results in a dramatic temperature drop of the PV cells and thus tremendously benefits their selection, lifetime and conversion efficiencies, enabling higher system efficiency and lower cost.

Integrating the two technologies introduced above, that solar thermochemistry and solar spectral filter, would be a further attempt for higher energy conversion efficiency. Stojanoff mentioned in his work that the thermal energy from a spectral splitting-based CPVT system can be used as chemical energy storage [27]. However, no specific method was suggested. In 1997, Lassich registered a patent for a spectral-splitting system to generate hydrogen by electrolysis [28]. Zamfirescu proposed a solar tower concentrating system to realize hydrogen production (water photolysis), PV power generation and Rankine power generation using different wavelengths via spectral filtering [29]. Li proposed a photovoltaic-methane-steam-reforming hybrid system by point-focus concentration and spectral splitting for heat and power cogeneration [30,31]. However, no study has examined the use of thermal energy from a spectrally selective filtered CPVT system to drive methanol-based thermochemistry.

Methanol has been of great interest in recent years, and many researchers consider it as an ideal energy carrier during the transition period from traditional energy to clean energy, for its high energy density, easy storage and shipment, and compatibility to the present infrastructures. Shih termed methanol as "liquid sunshine" for its huge potential in harvesting and storing solar energy [32]. Verhelst reviewed methanol's performance as an alternative fuel for internal combustion engines and substantiated its capability in transportation sector [33]. In fact, many developing countries are deploying projects based on methanol economy, such as China's M100 methanol vehicle pilot program [34] and India's Methanol Economy Fund [35]. Except for transportation sector, methanol is also capable of powering distributed energy system as a convenient energy carrier. During this process, methanol thermochemistry driven by concentrated solar energy has been verified as a potential route towards further increases in efficiency, as discussed in the second paragraph in this part.

In this paper, we propose a novel CPVT system that combines spectral filtering technique and methanol-decomposition thermochemistry. Compared with conventional spectral-splitting CPVT systems [24,27,28], methanol decomposition is incorporated for the first time. Thermodynamic calculation, coupling solar PV and solar thermal, is carried out to figure out the optimal energy allocation scheme between PV and thermal. Based on the thermodynamic results, we design the optical model with detailed linear Fresnel reflectors layout and suitable spectral filter. To further demonstrate the applicability of the proposed system from a practical point of view, sensitivity analysis and cost analysis are also performed, to examine whether the efficiency loss and cost increase caused by high systematic complexity (compared with regular CPVT systems) could be offset by efficiency gain.

2. System description

Fig. 1(a) shows the photovoltaic-thermochemical system conceptually. Compared with conventional linear concentrating solar thermal systems, a spectral filter and PV modules are proposed in addition to the tubular solar thermal receiver. The PV cell is chosen as CdTe thin film cell whose favorable spectrum that allows PV generation at high efficiency ranges from 400 to 800 nm [36]. As shown in Fig. 2, the external quantum efficiency maintains at high level for the wavelength within 400–800 nm for a typical CdTe cell, so that the filter transmits 400–800 nm section of the solar spectrum for solar PV and reflects the remainder for solar thermal. In Fig. 1(a), green arrows indicate mass flow: liquid methanol is preheated to its gaseous state by residual heat from the PV modules, converted into syngas by the heat directly supplied from the solar thermal receiver, and lastly the syngas fuel is delivered to a

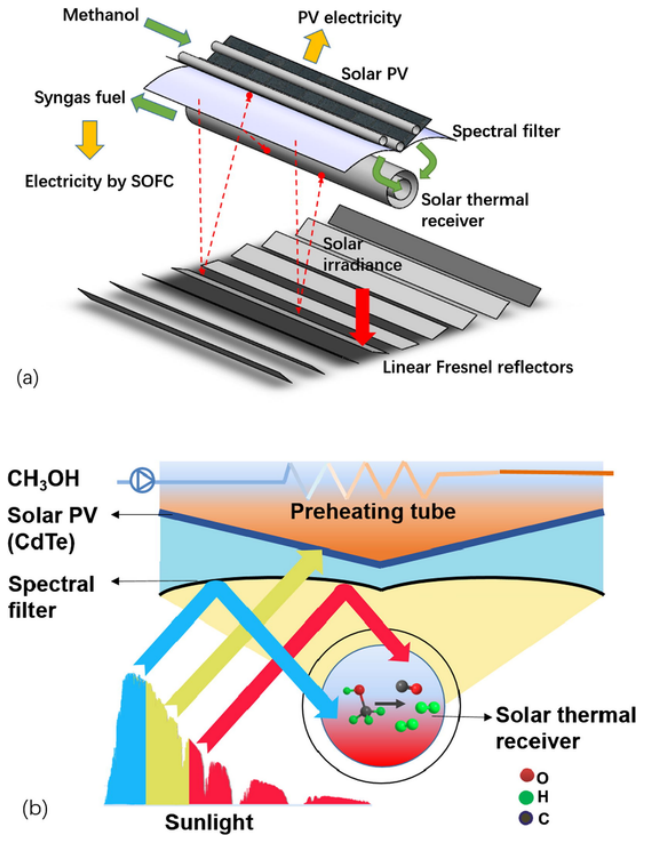

Fig. 1. (a) Schematic diagram of the concentrated photovoltaic thermal system. Green arrows indicate mass flow: liquid methanol is preheated by PV residual heat, then converted into syngas by the solar thermal heat, and lastly the syngas fuel is delivered to a solid oxide fuel cell system. Yellow arrows electricity outputs. Red arrows indicate optical path: sunlight is concentrated by linear Fresnel reflectors towards both the solar thermal receiver and the filter, and the filter reassigns the spectra to different working sectors. (b) Cross-sectional structure of key components. 400–800 nm spectra transmit the filter onto solar PV and the remainder is reflected back onto solar thermal for methanol decomposition. (For interpretation of the references to colour in this figure legend, the reader is referred to the web version of this article.)

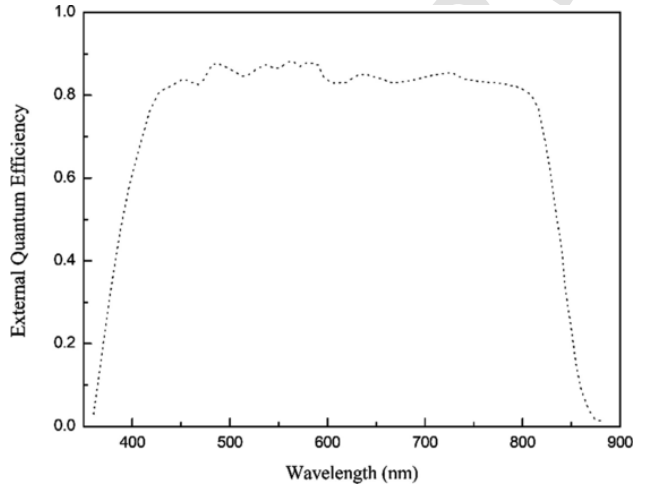

Fig. 2. External quantum efficiency of CdS/CdTe solar cell with 30 nm CdS layer. Data from [36].

solid oxide fuel cell (SOFC) system to generate electricity. Yellow arrows indicate electricity outputs. Red arrows indicate optical path: sunlight is concentrated by linear Fresnel reflectors towards both the solar thermal receiver and the filter, and the filter reassigns the concentrated sunlight to different working sectors, i.e. 400–800 nm for solar PV and the rest for solar thermal. Note that there is still a portion of sunlight directly reflected onto the receiver and the proportion is adjustable by manipulating Fresnel reflectors' tilt angles (see Table 1).

Fig. 1(b) displays the cross-sectional structure of some key components to demonstrate the optical path in depth. For the sunlight that reaches the filter, 400–800 nm spectrum transmit through the filter onto solar PV, and the rest is reflected back onto the solar thermal receiver for methanol decomposition (reaction equation by R1). In other words, the filter also acts as a secondary concentrator for solar thermochemistry. With a secondary concentrator, working temperature of solar thermal could easily exceed 200 °C, that matches the reaction temperature with $CuO/ZnO/Al_2O_3$ catalyst.

$$CH_3OH(g) \rightarrow CO(g) + 2H_2(g) \quad \text{(R1)}$$

3. Model

3.1. Thermodynamic model

One particular challenge for a spectrally selective CPVT system is the matching between the energy demand and supply for both the PV side and thermal side. Specifically, with a fixed spectrum allocation scheme to both sides, the PV waste heat provides a given amount of thermal energy for preheating a certain amount of methanol for vaporization, whereas the direct solar thermal heat supply might decompose a different amount of methanol. Due to the different characteristics of solar PV cells, the cutoff threshold for spectral filtering varies, and thus the two amounts may be largely independent of each other. Therefore, thermodynamic calculation coupling solar PV and solar thermal would be necessary, in order to figure out the intrinsic relevance between system efficiency and energy allocation ratio between PV and thermal.

A dimensionless thermodynamic model is built as shown in Fig. 3. The control volume encloses solar PV modules and solar thermal receiver. The energy input is solar energy concentrated by Fresnel reflectors, where a portion of sunlight is directly reflected onto the receiver and this portion is defined as x. The rest of concentrated sunlight ($1-x$) that reaches the filter is split into two different directions towards PV and

Table 1
System parameters of the spectral-splitting CPVT system.

Parameters	Value
DNI	1000 W/m ^{2}
Reaction temperature	220 °C
Transmitted wavelength of the filter	400–800 nm
Optical efficiency	75%
PV concentration ratio	33
Thermal concentration ratio	50
PV peak efficiency	22% [37]
PV temperature coefficient	−0.25% [38]
SOFC efficiency	50–70% [39], taken as 50%

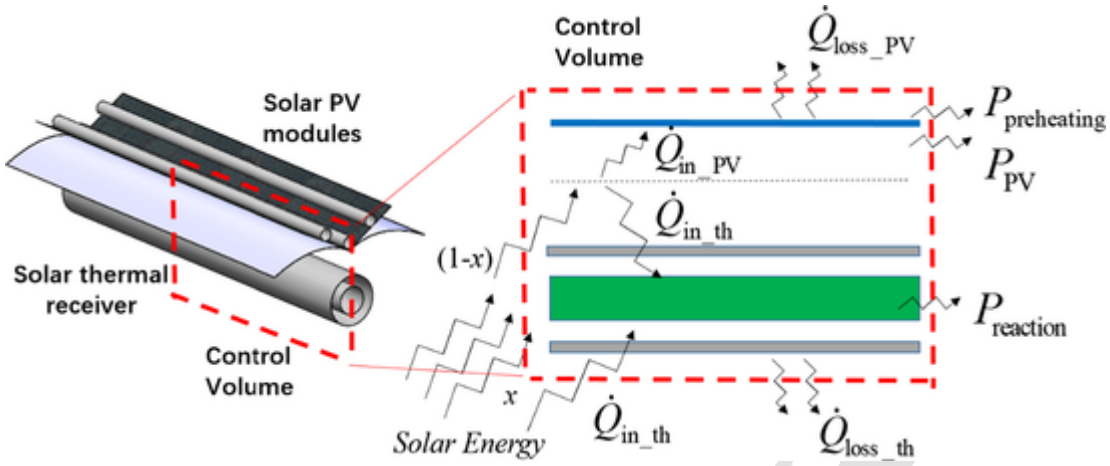

Fig. 3. Schematic energy flow chart and balance in the control volume.

thermal components. Energy outputs include methanol preheating power, PV power and methanol decomposition power. Heat losses involve those by both solar PV and solar thermal parts, mainly via convection and radiation. The detailed parameters are explicated as follows, and the values are listed in Tab. 1.

The input solar energy rate onto PV modules is calculated by the following:

$$\dot{Q}_{\text{in\_PV}} = A_{\text{pri}} \cdot \eta_{\text{opt}} \cdot (1 - x) \cdot \int_{400\text{nm}}^{800\text{nm}} DNI(\lambda)\, d\lambda \tag{1}$$

where A_{pri} is the total area of the primary Fresnel reflectors, $DNI(\lambda)$ refers to the literature [40], x is the proportion of the primarily reflected solar flux trapped by the receiver, and η_{opt} is the optical efficiency.

The input solar energy rate to the thermal part includes two parts, the direct flux onto the receiver after the primary reflection and the flux reflected by the filter after the secondary reflection, which is given by the following:

$$\dot{Q}_{\text{in\_th}} = A_{\text{pri}} \cdot \eta_{\text{opt}} \left[\left(DNI - \int_{400\text{nm}}^{800\text{nm}} DNI(\lambda)\, d\lambda \right) \cdot (1 - x) + DNI \cdot x \right] \tag{2}$$

The heat loss rates of solar PV modules and the solar thermal receiver are given by the following:

$$\dot{Q}_{\text{loss\_PV}} = A_{\text{PV}} \cdot \left[h \cdot (T_{\text{PV}} - T_{\text{amb}}) + \sigma \cdot \varepsilon_{\text{PV}} \cdot (T_{\text{PV}}^4 - T_{\text{amb}}^4) \right] \tag{3}$$

$$\dot{Q}_{\text{loss\_th}} = A_{\text{th}} \cdot \left[h \cdot (T_{\text{th}} - T_{\text{amb}}) + \sigma \cdot \varepsilon_{\text{th}} \cdot (T_{\text{th}}^4 - T_{\text{amb}}^4) \right] \tag{4}$$

where the subscript amb denotes the ambient, th denotes the thermal receiver, h is the convective coefficient, ε is the emissivity, and A represents the area.

For PV electricity output, we assume that the spectrum range of 400–800 nm generates the same amount of electricity as the full spectrum incidence and only consider the temperature effect on the PV efficiency [38]. Thus, the PV power generation output is given by the following:

$$P_{\text{PV}} = 0.22 A_{\text{pri}} \cdot \eta_{\text{opt}} \cdot (1 - x) \cdot \left[1 - 0.0025 \left(T_{\text{PV}} - T_{\text{amb}} \right) \right] \tag{5}$$

Residue heat from PV modules is utilized for methanol gasification, and the preheating power is calculated by:

$$P_{\text{preheating}} = \left(\int_{T_{\text{amb}}}^{T_{\text{bp}}} C_p dT + H + \int_{T_{\text{bp}}}^{T_{\text{pre}}} C_p dT \right) \cdot \dot{m} \tag{6}$$

where C_P represents the specific heat capacity of methanol, T_{bp} denotes the boiling point of methanol, T_{pre} denotes the outlet temperature of the preheated methanol, which is assumed to be 5 °C lower than PV temperature. H is the latent heat of methanol, $\dot{m}$ stands for methanol mass flow rate.

The thermal power required for reaction is calculated by the

following:

$$P_{\text{reaction}} = \left(\int_{T_{\text{pre}}}^{T_{\text{th}}} C_p dT + y \cdot E \right) \cdot \dot{m} \tag{7}$$

where T_{th} is the reaction temperature, T_{pre} denotes the outlet temperature of the preheated methanol, y represents the conversion rate of methanol decomposition reaction, E denotes the endothermic heat of the reaction.

In this specific system, the thermal energy is utilized in two separate parts: the PV heat for fuel preheating and the high temperature heat for fuel decomposition. To ensure a unified mass flow rate, the mass flow rate $\dot{m}$ is calculated by solving the following:

$$\dot{m} = \frac{\dot{Q}_{\text{in\_PV}} - \dot{Q}_{\text{loss\_PV}} - P_{\text{PV}}}{\int_{T_{\text{en}}}^{T_{\text{pre}}} C_p dT + H + \int_{T_{\text{bp}}}^{T_{\text{pre}}} C_p dT} = \frac{\dot{Q}_{\text{in\_th}} - \dot{Q}_{\text{loss\_th}}}{\int_{T_{\text{pre}}}^{T_{\text{th}}} C_p dT + y \cdot E} \tag{8}$$

The work capacity of fuel can be evaluated as the electricity output by utilizing syngas through a SOFC system. We can calculate the solar energy proportion of the syngas fuel by subtracting the methanol-contributed electricity output of SOFC. Thus, the electricity output of SOFC contributed by solar energy is given by the following:

$$P_{\text{th}} = \Delta H \cdot y \cdot \dot{m} \cdot \eta_{\text{SOFC}} \tag{9}$$

where ΔH denotes the heating value difference per kilogram between methanol and that of syngas decomposed by the same amount of methanol and η_{SOFC} represents the efficiency of the SOFC system.

Then, the net solar-to-electric efficiency of this system can be obtained by the following formula:

$$\eta_{\text{NSE}} = \frac{P_{\text{PV}} + P_{\text{th}}}{DNI \cdot A_{\text{pri}}} \tag{10}$$

To further evaluate the energy storage capacity of the hybrid system, the thermochemical efficiency is defined as the ratio of the additional chemical energy stored in the syngas to the total thermal energy received by the CPVT system:

$$\eta_{\text{th-chem}} = \frac{E \cdot y \cdot \dot{m}}{\dot{Q}_{\text{in\_th}} + \dot{Q}_{\text{in\_PV}} - P_{\text{PV}}} \tag{11}$$

3.2. Optical model

In this paper, the use of Fresnel reflectors increases the flexibility of designing the energy-allocation scheme via adjusting the proportion of the energy received by the solar thermal receiver versus that by the PV modules. This adjustment is achieved by appointing specific mirrors to reflect sunlight towards either the receiver or the PV modules. In turn, the energy demand and supply can be balanced.

To verify the feasibility of the strategy above, especially on how solar energy can be concentrated and allocated. A two-dimensional optical model is established using the Monte Carlo method. In this symmetrical model, as shown in Fig. 4, the receiver is placed at a height of 4 m with a radius of 0.068 m. The overall reflector field requires 68 mirrors, each with a width of 0.1 m. PV modules are placed over the filter, with a width on each side of 0.096 m. The layout of each Fresnel mirror and the geometry of the filter will significantly affect the energy allocation, and at the first stage, all of these parameters cannot be ascertained. We assume the filter's curve as a parabola and the given values for the mirrors' tilt angles to achieve a vague scope of energy allocation; this allocation will be useful for the initial thermodynamic model design. In turn, based on the final thermodynamic results obtained by iteration, the modified optical geometric parameters can be calculated. The spectrum distinction of sunlight is simplified as the energy proportion in this model. For example, we consider the 400–800 nm wave range as 54.2% of the full spectrum from an energy proportion view, neglecting their quantum difference.

3.3. Validation

For the two models above, calculation results could be a strong function of some key parameters, such as heat loss coefficient, reaction thermodynamics, concentrating and filtering characteristics. With these parameters calibrated by experimental data, the credibility of the models would be significantly enhanced. In this part, calibrations for key parameters are performed to validate both the thermodynamic model and the optical model.

Numerous numerical and experimental studies on methanol-based solar thermochemistry have been performed in terms of methanol decomposition within a solar thermal receiver [14,41,42,43], and considerable validation work has been done. The solar thermal receiver and the reaction system are modeled in a manner similar to our previous work. So

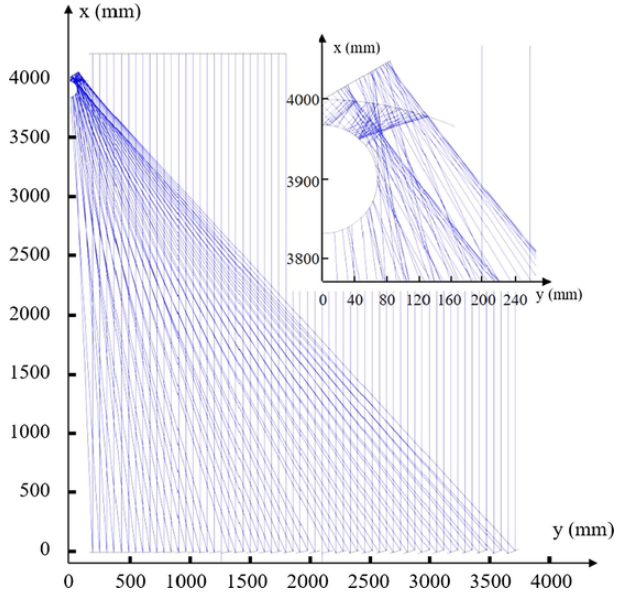

Fig. 4. Optical model of the system. Details of filter, receiver and PV are displayed in the top-right with enlarged scale.

in the thermodynamic model, we apply the calibrated parameters from our previous work, i.e. heat loss coefficient from [43] and reaction thermodynamics from [17].

In contrast, the employment of linear Fresnel reflectors and spectral filter in this study is a new attempt. We validate the optical model by comparing concentrated solar flux on the focal plane against that in the literature [44]; and calibrate the spectral filter's optical property by a real filter's measured data. For the optical model, we set the same parameter input as that in the literature [44], calibrated the model's grid, and obtained the distribution of concentrated solar flux on the focal plane (Fig. 5). The results are in good agreement with that in the literature, thereby indicating that the optical model is reliable. For the spectral filter's optical property, Fig. 6 gives two transmittance curves of the designed spectral filter, i.e. one by simulation and the other by measurement. The target transmittance for transition band (400–800 nm) is 0.9–1, and the filtering characteristic shown in Fig. 6 verifies the feasibility of our spectral design. Besides, the overall transmittance for the range of 400–800 nm is taken as 0.9, and this calibrated value is multiplied with the existing optical efficiency.

4. Results and discussion

4.1. Net Solar-to-Electric (NSE) efficiency with different energy allocation

Fig. 7 shows the net solar-to-electric efficiency of the system with different allocation ratio of solar energy (i.e. primary reflection design) and the corresponding contributions from the PV modules and thermochemistry system. Allocation ratio is defined as the ratio of the total solar energy that arrives at the surface of solar thermal receiver to that arrives at the surface of PV modules. The ratio is adjustable by manipulating specific mirrors' tilt angles. The results show that the peak NSE efficiency reaches 39.4% when the allocation ratio is around 1.6, which could be considered as the optimal ratio. When the proportion of solar thermal increases, the solar thermal electricity maintains a stable output, and the PV electricity output increases first and then decreases slightly, and this trend will be explained in detail in the following chapters. Thus, the

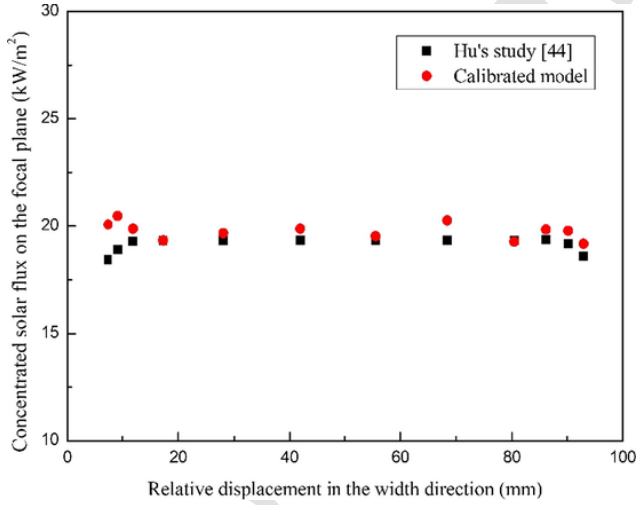

Fig. 5. Concentrated solar flux on the focal plane, compared with [44]. The optical model set the same parameter input as [44]. (Grid number of the concentrator: 1000; tilt angle of the focal plane: 30°; mirror number: 20; solar irradiance: 1000 kW/m^2).

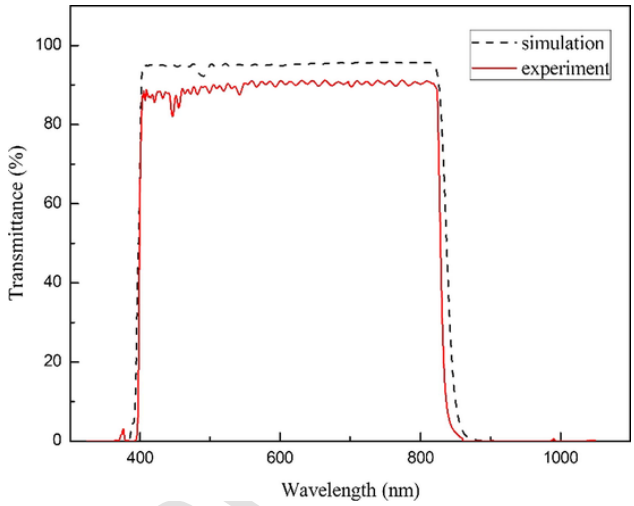

Fig. 6. Transmittance as a function of wavelength of the designed spectral filter. Black line stands for simulation result: the filter is designed with 70 layers of Ta_2O_5/SiO_2 ($n_H = 2.27$, $n_L = 1.48$) coating system, simulated by Essential Macleod [45]. Red line stands for experimental result: a real filter is manufactured via physical vapor deposition technique provided by Shenyang Academy of Instrumentation Science Co. Ltd, and the transmittance is measured within normal incidence by a spectrophotometer (Agilent CARY 6000). (For interpretation of the references to colour in this figure legend, the reader is referred to the web version of this article.)

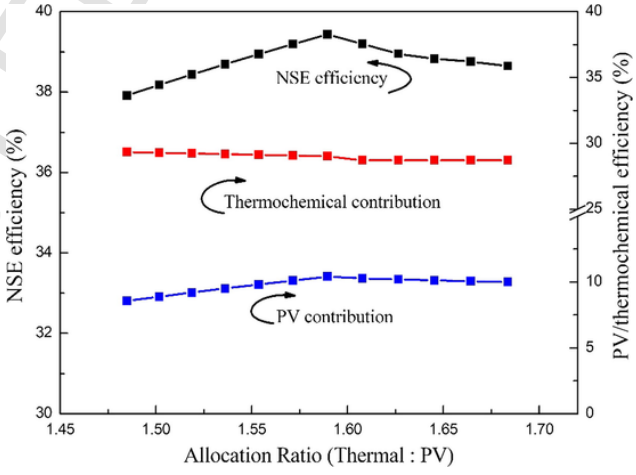

Fig. 7. NSE efficiency with different allocation ratios (Solar thermal versus Solar PV).

NSE efficiency shows the same trend as the PV electricity output, and there exists a peak NSE efficiency with different primary reflected energy allocations. This optimal allocation ratio is exclusive to this system due to the intrinsic property of methanol and CdTe cell, while the methodology could be applied to this kind of CPVT systems in general.

4.2. Optical design within the optimal energy allocation scheme

As mentioned above, energy allocation ratio is dependent on primary reflection design, so we modified the optical model to validate the optimal energy allocation scheme above. In order to obtain the allocation ratio of 1.6, the filter's geometric shape and the mirrors' tilt angle are designed as follows. The cross-sectional curve of the filter on the right hand side can be expressed as Eq. (12), and mirror tilt angles on the same

side are given in Table 2. The left hand side is symmetrical, for both the curve and mirror layout.

$$y = -\frac{1}{800}x^2 + 4000 (0<x<165) \quad (12)$$

Fig. 8 gives the solar flux distribution onto the PV module's and the receiver's surfaces, as calculated from the optical model. After the primary reflection by linear Fresnel mirrors, a part of the concentrated sunlight hits the bottom of the solar thermal receiver, with an average concentration ratio of 7.6. The rest that goes for the filter is split afterwards, and directed towards the receiver's top surface and PV module's surface, with average concentration ratios of 9.9 and 12.1, respectively. By integrating the solar flux in Fig. 8 with the corresponding area, the total energy input towards different sectors can be obtained, and in turn the allocation ratio is available. For this specific optical design, the energy allocation ratio exactly meets the optimal allocation scheme as discussed above. Note that the concentration ratio in this part refers to flux concentration ratio, whose value varies with geometric concentration ratio due to optical loss and spectral filtering. In this case, the flux concentration ratio of 17.5 (7.6 + 9.9) is sufficient to heat up a tubular solar thermal receiver to 220 °C, with the calibrated heat transfer coefficient from [17,43].

4.3. PV performance

Fig. 9 shows the PV working conversion efficiency and the PV electricity output per unit solar collecting area under different energy allocation ratios. Compared with a nonfilter CPVT system that uses the PV waste heat to drive the reaction, such as our previous system in [17], the PV temperature drops by over 100 °C. This improvement in PV operating condition results from the allocation of suitable wavelengths to PV cells, thereby alleviating its heating effect. As the proportion of solar flux onto the thermal receiver increases, the PV conversion efficiency first increases and then remains at a constant value. This phenomenon occurs because when the allocation ratio (thermal versus PV) is over 1.6, the input solar energy to the fuel preheater is no longer sufficient for total methanol gasification, and the heating burden is partially shifted to the receiver. Consequently, the PV cells will remain at 70 °C (5 °C higher than the methanol boiling point), with a stable conversion efficiency of 19.4%. However, this allocation scheme is slightly detrimental to PV power generation because the reduced irradiance onto the PV cells with a constant conversion efficiency results in a decreased PV power output.

4.4. Thermochemical performance

Thermochemical efficiency embodies the energy storage capacity of the hybrid system, which has been defined previously in Section 2. The thermochemical efficiency is maintained at a high level (60–65%), indicating that nearly two-thirds of the thermal energy captured by the system can be stored via syngas, which can be fed into the SOFC to supply electricity when sunlight is absent. This energy storage ratio is even higher than that of our previous GaAs-based system (45%) [16] because the conversion efficiency of the CdTe cell is lower than that of the GaAs cell. That is, more solar energy is used to drive the chemical reaction, resulting in a higher percentage of solar energy storage in the syngas rather than direct conversion to electricity.

4.5. Sensitivity analysis

In this part, we analyze the influence of non-ideal operating conditions on system efficiency, since in practice, it is virtually impossible for the system to work under optimum conditions. Various undesirable factors, such as unstable solar radiation, may seriously impact the performance of the system. Therefore, it is important to perform a sensitivity analysis to evaluate the overall system. In addition, different concentration ratios for thermochemical parts are included to test the system's response capacity against these non-ideal conditions.

Fig. 10(a) shows the influence of the PV cells' efficiency on the NSE efficiency of the system. In the case studied above, we assumed that the transmitted spectrum (400–800 nm) onto the PV cell generates the same amount of electricity as the full spectrum incidence because the CdTe cell's favorable solar spectrum with high external quantum efficiency ranges from 400 to 800 nm. Now we consider a real operating condition in which the PV cell can only generate electricity with a part of the solar spectrum, while the rest of the spectrum is converted into heat instead. We define a factor η as follows

$$\eta = \frac{P_{PV,\ 400-800\ nm}}{P_{PV,\ full\ spectrum\ incidence}} \quad (13)$$

where the numerator represents the PV electricity generated by wavelengths of 400–800 nm and the denominator represents the PV electricity generated by full-spectrum solar irradiation. The results show that when η decreases from 0.95 to 0.85, the NSE efficiency drops from 39.1% to 38.4% with a concentration ratio of 50, and the same trends hold under a

Table 2
Mirror tilt angles on the right side.

No.	Tilt angle (°)	No.	Tilt angle (°)	No.	Tilt angle (°)	No.	Tilt angle (°)
1	1.2069	10	6.8858	19	12.6260	28	17.9655
2	1.8200	11	7.5296	20	13.2465	29	18.5187
3	2.4390	12	8.1735	21	13.8612	30	19.0629
4	3.0633	13	8.8168	22	14.4698	31	19.5977
5	3.6923	14	9.4588	23	15.0716	32	20.1230
6	4.3254	15	10.0988	24	15.6663	33	20.6387
7	4.9619	16	10.7362	25	16.2534	34	21.1446
8	5.6013	17	11.3703	26	16.8325		
9	6.2428	18	12.0004	27	17.4033		

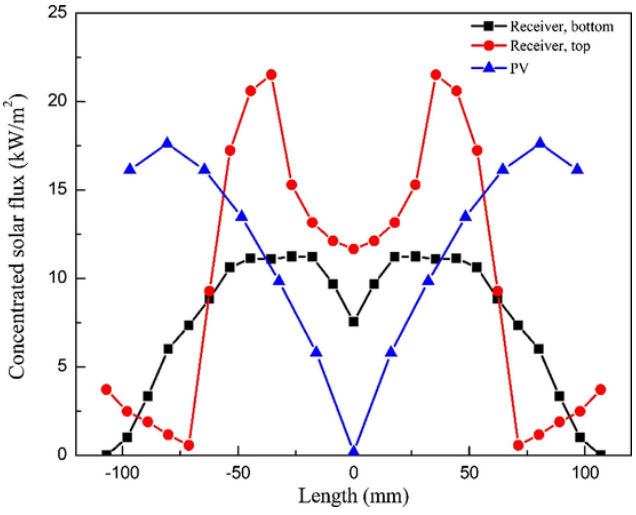

Fig. 8. Concentrated solar flux distribution on the PV module (x-axis represents PV length) and thermal receiver (x-axis represents receiver's arc length).

concentration ratio from 50 to 70, as shown in Fig. 10(a). Obviously, when PV cells generate less electricity and more thermal energy, the system's NSE efficiency decreases, but the change in NSE efficiency is relatively slow compared with the corresponding change in the PV cells' efficiency. This feature is a benefit of the methanol preheating design, which allows the PV-dissipated heat to be recovered. If η is decreased to zero, the NSE efficiency will be equivalent to that of the solar thermochemical system without PV cells [14]. From this comparison, we conclude that the hybrid system can always achieve superior NSE efficiency compared with pure thermochemical systems with identical conditions of the methanol reaction part.

Fig. 10(b) displays the impact of the DNI on the NSE efficiency. In the previous case, we ideally took the solar radiation as 1000 W/m^2. Now, we set DNI in a range from 400 to 1000 W/m^2 and calculate the NSE efficiencies under the corresponding sunlight conditions. The results show that the NSE efficiency remains over 39% with different concentration ratios as long as the DNI is over 800 W/m^2. This result occurs because we can always obtain the optimal working condition even with different DNI conditions by manipulating the Fresnel reflectors to achieve the optimum primary reflection allocation and further maintain the system at high efficiency. However, the decrease in NSE efficiency becomes serious when the DNI drops to 400 W/m^2 because the heat loss remains while the solar input decreases significantly, and therefore the NSE efficiency drops sharply.

In conclusion, the degradation of PV and unstable sunlight input may negatively impact the system, but the sensitivity analysis shows that the system's NSE efficiency will remain at a high level (over 37%) in a practical sense, in most of the non-ideal conditions.

4.6. Cost analysis

The economic analysis is performed for a prototype system with a sunlight-collecting area of 100 m^2. Table 3 lists the detailed operating conditions and estimated cost of the system. Linear Fresnel reflector concentration is a cost-effective solar concentration approach, with a cost of approximately \$100/m^2 (collecting area), including receivers, mirrors and other accessories [46]. For the PV cells, with the rapid development of CdTe cells, especially by some leading companies such as First Solar, the cost of CdTe PV cells is as low as \$72/m^2 [47]. Compared with these two components above, the unit cost of the spectral filter unit area is higher. The average price for the filter with the aforementioned optical characteristics, based on the manufacturers specifications, is as high as \$1000/m^2. However, with the secondary reflector design, only 3 m^2 is needed for the spectal-splitting device, and the capital cost of the filter for this system is therefore \$3000. SOFC represents the largest proportion of the capital investment. According to an annual report from DOE, the cost of an SOFC ranges from \$787 to \$1194 per kW electricity [48]. Therefore, we take a reasonable value of \$1000/kW and obtain the SOFC's capital cost as \$170,400. Additionally, the cost of accessories (e.g., valves, joints, pipelines, etc.) is assumed to be \$2000. Thus, the total capital cost for this solar plant is estimated to

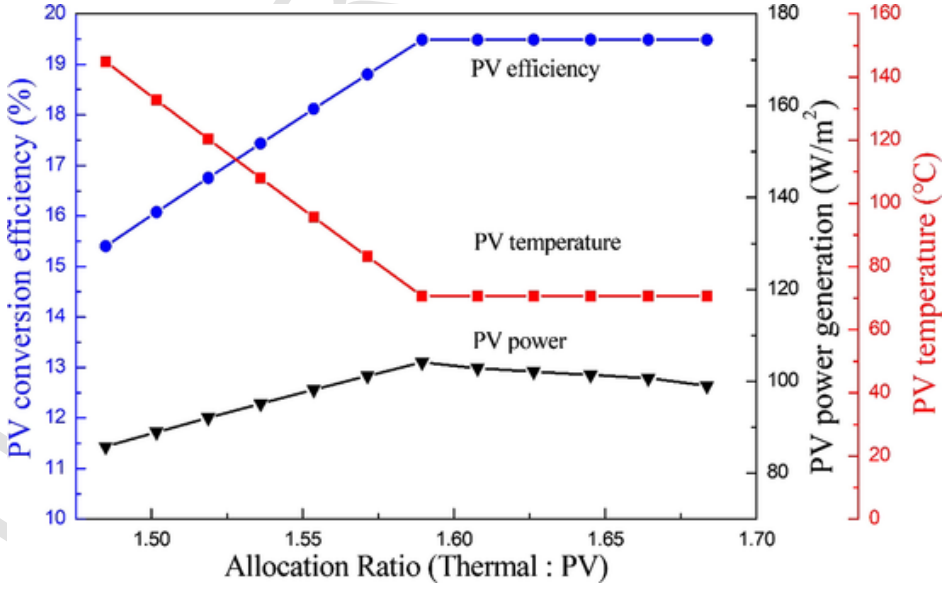

Fig. 9. PV performance of the system under different energy allocation ratio (Solar thermal versus Solar PV).

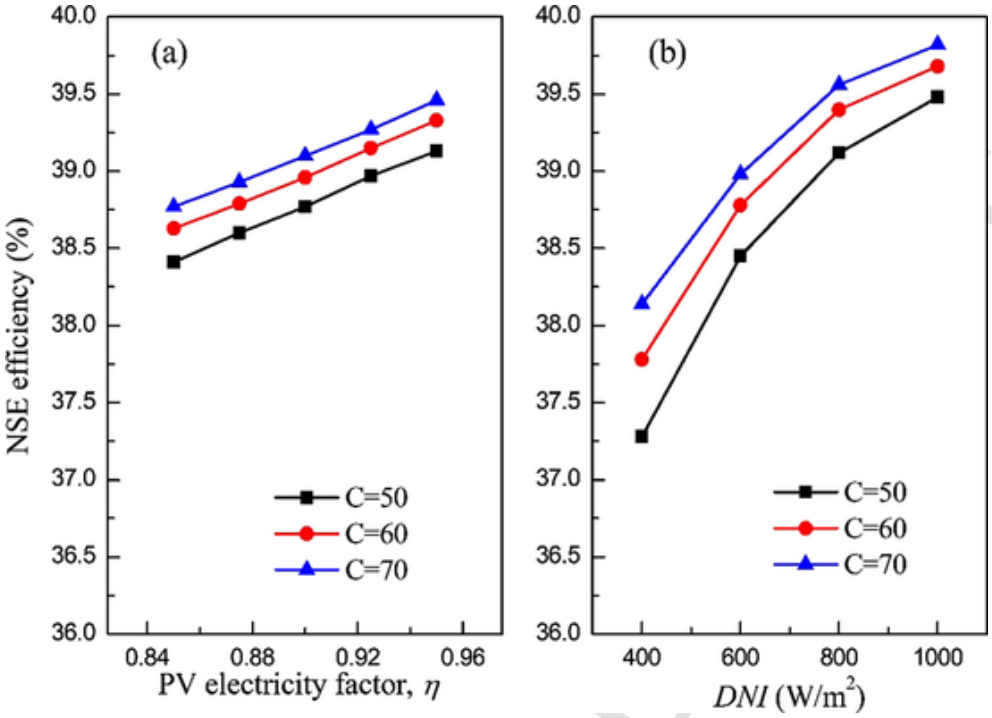

Fig. 10. Sensitivity analysis for non-ideal operating conditions.

Table 3
Estimated levelized cost of electricity (LCOE) of the system.

Parameters	Value
Plant size, energy, and mass flow	
Fresnel reflector area	100 m^2
Solar input on reflector	200 MWh/yr
Methanol requirement	102 tons/yr
Syngas production (LHV)	681 MWh/yr
Electricity output by fuel cell	340 MWh/yr
Electricity output by PV cell	20 MWh/yr
Total electricity production	360 MWh/yr
Capital cost	
Collector + receiver	$10,000
CdTe PV cell	$218
Filter	$3000
SOFC	$170,400
Other	$2000
Total capital cost	$185,618
Annual cost	
Annual fixed interest rate	5%
Operation & Maintenance rate	2%
Methanol	$40,896 /yr
Total annual cost	$44,608 /yr
Specific cost	
LCOE	$0.20/kWh

be $185,618. An annual fixed charge rate of 5% is assumed, and the operation & maintenance rate is taken as 2%. The methanol price is obtained from Methanex [49], and $40,896 is needed per year for 102 tons of methanol as feedstock. Thus, the annual operation cost totals $44,608.

The levelized cost of electricity (LCOE) is calculated by:

$$LCOE = \frac{f_{CR} \cdot C_{TC} + C_{O\&M} + C_{Methanol}}{E_{annual}} \quad (14)$$

where f_{CR} is capital recovery factor, C_{TC} denotes total capital cost, $C_{O\&M}$ is annual cost of operation and maintenance, $C_{Methanol}$ represents annual methanol cost and E_{annual} is annual electricity production. Capital recovery factor can be calculated by:

$$f_{CR} = \frac{i \cdot (1+i)^n}{(1+i)^n - 1} \quad (15)$$

where i is annual fixed interest rate and n is investment payback period.

The LCOE of this prototype system is estimated to be $0.20/kWh, assuming a ten-year investment payback period. This value accounts all the materials input including annual feedstock like methanol, and accounts the total electricity output, including both solar-contributed and chemical-contributed electricity. As stable electricity output is crucial in practice, which capability our system features by syngas storage, the reference PV power system is chosen as PV-battery combined power systems with energy storage capability. Though the PV electricity cost has been as down as $0.1/kWh [50], the cost for battery energy storage remains high ($0.8–1.0/kWh) [51], which makes PV-battery combined power systems at a disadvantage in cost. Indeed, the cost of this CPVT system is competitive with those of electricity generated via solar thermal routes ($0.27/kWh) [50], provided that they are constrained to similar annual solar irradiation conditions. Compared with methanol-based solar thermochemical systems, our cost-effective PV cells and filtering design not only bring about great advancements in NSE efficiency but also avoid an increase in unit power cost. Moreover, as the scale increases, the cost of the hybrid system will be further reduced in the future.

5. Conclusion

A concentrated PV-thermal (CPVT) system featuring controllable allocation of photonic solar energy between PV and thermochemical modules is presented. The allocation is enabled by the adoption of both a spectral filter and linear Fresnel reflectors, and the thermochemical module based on methanol decomposition provides a strong basis for net solar-to-electric (NSE) efficiency at the system level. With a CdTe cell as the PV component, the system-level NSE efficiency is as high as 39%, and the solar thermal energy storage efficiency is over 60%. Both of these improvements are due to the dramatic decrease in PV temperature induced by spectral filtering, as well as the "double-heat-source" design, which effectively preheats and decomposes methanol in different parts of the system. Sensitivity and cost analyses verify the feasibility of this system, with an NSE efficiency of 37–38% under non-ideal working conditions and a specific cost of solar electricity as low as $0.20/kWh. The high efficiency and great potentials for cost reduction might enable further advances in PVT technologies.

References

[1] TT Chow. A review on photovoltaic/thermal hybrid solar technology. Appl Energy 2010;87:365–379.

[2] HA Zondag, DW de Vries, WGJ van Helden, RJC van Zolingen, AA van Steenhoven. The yield of different combined PV-thermal collector designs. Sol Energy 2003;74:253–269.

[3] W He, J Zhou, C Chen, J Ji. Experimental study and performance analysis of a thermoelectric cooling and heating system driven by a photovoltaic/thermal system in summer and winter operation modes. Energy Convers Manage 2014;84:41–49.

[4] OZ Sharaf, MF Orhan. Concentrated photovoltaic thermal (CPVT) solar collector systems: Part I – Fundamentals, design considerations and current technologies. Renew Sustain Energy Rev 2015;50:1500–1565.

[5] OZ Sharaf, MF Orhan. Concentrated photovoltaic thermal (CPVT) solar collector systems: Part II – Implemented systems, performance assessment, and future directions. Renew Sustain Energy Rev 2015;50:1566–1633.

[6] G Kosmadakis, D Manolakos, G Papadakis. Simulation and economic analysis of a CPV/thermal system coupled with an organic Rankine cycle for increased power generation. Sol Energy 2011;85:308–324.

[7] A Moaleman, A Kasaeian, M Aramesh, O Mahian, L Sahota, TG Nath. Simulation of the performance of a solar concentrating photovoltaic-thermal collector, applied in a combined cooling heating and power generation system. Energy Convers Manage 2018;160:191–208.

[8] G Mittelman, A Kribus, O Mouchtar, A Dayan. Water desalination with concentrating photovoltaic/thermal (CPVT) systems. Sol Energy 2009;83:1322–1334.

[9] A Al-Alili, Y Hwang, R Radermacher, I Kubo. A high efficiency solar air conditioner using concentrating photovoltaic/thermal collectors. Appl Energy 2012;93:138–147.

[10] G Mittelman, A Kribus, A Dayan. Solar cooling with concentrating photovoltaic/thermal (CPVT) systems. Energy Convers Manage 2007;48:2481–2490.

[11] Z Xu, C Kleinstreuer. Concentration photovoltaic–thermal energy co-generation system using nanofluids for cooling and heating. Energy Convers Manage 2014;87:504–512.

[12] M Li, X Ji, GL Li, ZM Yang, SX Wei, LL Wang. Performance investigation and optimization of the Trough Concentrating Photovoltaic/Thermal system. Sol Energy 2011;85:1028–1034.

[13] RM da Silva, JLM Fernandes. Hybrid photovoltaic/thermal (PV/T) solar systems simulation with Simulink/Matlab. Sol Energy 2010;84:1985–1996.

[14] H Hong, H Jin, J Ji, Z Wang, R Cai. Solar thermal power cycle with integration of methanol decomposition and middle-temperature solar thermal energy. Sol Energy 2005;78:49–58.

[15] Q Liu, H Hong, J Yuan, H Jin, R Cai. Experimental investigation of hydrogen production integrated methanol steam reforming with middle-temperature solar thermal energy. Appl Energy 2009;86:155–162.

[16] W Li, Y Hao. Efficient solar power generation combining photovoltaics and mid-/low-temperature methanol thermochemistry. Appl Energy 2017;202:377–385.

[17] W Li, Y Ling, X Liu, Y Hao. Performance analysis of a photovoltaic-thermochemical hybrid system prototype. Appl Energy 2017;204:939–947.

[18] KAW Horowitz. A bottom-up cost analysis of a high concentration PV module. NREL; 2015.

[19] E Jackson. Areas for improvement of the semiconductor solar energy converter. Trans Intern Conf on the Use of Solar Energy-The Scientific Basis; 1955. p. 122.

[20] AG Imenes, DR Mills. Spectral beam splitting technology for increased conversion efficiency in solar concentrating systems: a review. Sol Energy Mater Sol Cells 2004;84:19–69.

[21] A Mojiri, R Taylor, E Thomsen, G Rosengarten. Spectral beam splitting for efficient conversion of solar energy—A review. Renew Sustain Energy Rev 2013;28:654–663.

[22] X Ju, C Xu, X Han, X Du, G Wei, Y Yang. A review of the concentrated photovoltaic/thermal (CPVT) hybrid solar systems based on the spectral beam splitting technology. Appl Energy 2017;187:534–563.

[23] A Segal, M Epstein, A Yogev. Hybrid concentrated photovoltaic and thermal power conversion at different spectral bands. Sol Energy 2004;76:591–601.

[24] Y Liu, P Hu, Q Zhang, Z Chen. Thermodynamic and optical analysis for a CPV/T hybrid system with beam splitter and fully tracked linear Fresnel reflector concentrator utilizing sloped panels. Sol Energy 2014;103:191–199.

[25] C Kandilli. Performance analysis of a novel concentrating photovoltaic combined system. Energy Convers Manage 2013;67:186–196.

[26] LA Weinstein, K McEnaney, E Strobach, S Yang, B Bhatia, L Zhao, et al. A hybrid electric and thermal solar receiver. Joule 2018;2:962–975.

[27] Froehlich K, Wagemann EU, Frohn B, Schulat J, Stojanoff CG. Development and fabrication of a hybrid holographic solar concentrator for concurrent generation of electricity and thermal utilization. In: Optical materials technology for energy efficiency and solar energy conversion XII: International Society for Optics and Photonics; 1993. p. 311–20.

[28] Lasich JB. Production of hydrogen from solar radiation at high efficiency. American Patents; 1997.
[29] C Zamfirescu, I Dincer. Assessment of a new integrated solar energy system for hydrogen production. Sol Energy 2014;107:700–713.
[30] W Li, J Jin, H Wang, X Wei, Y Ling, Y Hao, et al. Full-spectrum solar energy utilization integrating spectral splitting, photovoltaics and methane reforming. Energy Convers Manage 2018;173:602–612.
[31] W Li, H Wang, Y Hao. A PVTC system integrating photon-enhanced thermionic emission and methane reforming for efficient solar power generation. Sci Bull 2017;62:1380–1387.
[32] CF Shih, T Zhang, J Li, C Bai. Powering the future with liquid sunshine. Joule 2018;2:1925–1949.
[33] S Verhelst, JWG Turner, L Sileghem, J Vancoillie. Methanol as a fuel for internal combustion engines. Prog Energy Combust Sci 2019;70:43–88.
[34] Methanex. Methanex promotes safe methanol fuel use in China; 2015. <https://www.methanex.com/regional-news/china/methanex-promotes-safe-methanol-fueluse-china>.
[35] The Economic Times. Niti Aayog seeks Rs 5,000-crore methanol economy fund; 2017. <https://economictimes.indiatimes.com/news/economy/finance/niti-aayog-seeks-rs-5000-crore-methanol-economy-fund/articleshow/62141420.cms>.
[36] S Buecheler, L Kranz, J Perrenoud, AN Tiwari. CdTe Solar Cells. In: C Richter, D Lincot, CA Gueymard, editors. Solar energy. New York, NY: Springer; 2013. p. 1–28.
[37] Solar F. First Solar Series 4™ PV Module; 2017. <http://www.firstsolar.com/en/Modules/Series-4>.
[38] P Singh, NM Ravindra. Temperature dependence of solar cell performance—an analysis. Sol Energy Mater Sol Cells 2012;101:36–45.
[39] IEA Technology. Roadmap hydrogen and fuel. Cells 2015.
[40] CA Gueymard, D Myers, K Emery. Proposed reference irradiance spectra for solar energy systems testing. Sol Energy 2002;73:443–467.
[41] Z Hou, D Zheng, H Jin, J Sui. Performance analysis of non-isothermal solar reactors for methanol decomposition. Sol Energy 2007;81:415–423.
[42] J Sui, Q Liu, J Dang, D Guo, H Jin, J Ji. Experimental investigation of methanol decomposition with mid- and low-temperature solar thermal energy. Int J Energy Res 2011;35:61–67.
[43] Q Liu, Y Wang, J Lei, H Jin. Numerical investigation of the thermophysical characteristics of the mid-and-low temperature solar receiver/reactor for hydrogen production. Int J Heat Mass Transf 2016;97:379–390.
[44] P Hu, Q Zhang, Y Liu, C Sheng, X Cheng, Z Chen. Optical analysis of a hybrid solar concentrating Photovoltaic/Thermal (CPV/T) system with beam splitting technique. Sci China Technol Sci 2013;56:1387–1394.
[45] Macleod E. Thin Film Center Inc. <https://www.thinfilmcenter.com/essential.php>.
[46] A Rovira, R Barbero, MJ Montes, R Abbas, F Varela. Analysis and comparison of Integrated Solar Combined Cycles using parabolic troughs and linear Fresnel reflectors as concentrating systems. Appl Energy 2016;162:990–1000.
[47] Wikipedia. Cadmium telluride photovoltaics; 2019. <https://en.wikipedia.org/wiki/Cadmium_telluride_photovoltaics>.
[48] Contini V. Stationary and Emerging Market Fuel Cell System Cost Analysis–Primary Power and Combined Heat and Power Applications. 2016 DOE Annual Progress Report; 2016. <https://www.hydrogen.energy.gov/pdfs/progress16/v_f_7_contini_2016.pdf>.
[49] Methanex. Methanex posts regional contract methanol prices for North America, Europe and Asia; 2019. <https://www.methanex.com/our-business/pricing>.
[50] IRENA. Renewable Power Generation Costs in 2017; 2018.< https://www.irena.org/publications/2018/Jan/Renewable-power-generation-costs-in-2017>.
[51] N Lewis. Research opportunities to advance solar energy utilization. Science 2016;351:aad1920.